

Downward continuation and geoid determination based on band-limited airborne gravity data

P. Novák¹, B. Heck²

¹ Department of Geomatics Engineering, The University of Calgary, 2500 University Drive NW, Calgary, Canada T2N 1N4
e-mail: pnovak@ucalgary.ca; Tel.: +1 403 220 8794; Fax: +1 403 284 1980

² Geodetic Institute, University of Karlsruhe, Englerstrasse 7, 76128 Karlsruhe, Germany
e-mail: heck@gik.uni-karlsruhe.de; Tel.: +49 721 608 3674; Fax: +49 721 608 6808

Received: 6 June 2001 / Accepted: 3 January 2002

Abstract. The downward continuation of the harmonic disturbing gravity potential, derived at flight level from discrete observations of airborne gravity by the spherical Hotine integral, to the geoid is discussed. The initial-boundary-value approach, based on both the direct and inverse solution to Dirichlet's problem of potential theory, is used. Evaluation of the discretized Fredholm integral equation of the first kind and its inverse is numerically tested using synthetic airborne gravity data. Characteristics of the synthetic gravity data correspond to typical airborne data used for geoid determination today and in the foreseeable future: discrete gravity observations at a mean flight height of 2 to 6 km above mean sea level with minimum spatial resolution of 2.5 arcmin and a noise level of 1.5 mGal. Numerical results for both approaches are presented and discussed. The direct approach can successfully be used for the downward continuation of airborne potential without any numerical instabilities associated with the inverse approach. In addition to these two-step approaches, a one-step procedure is also discussed. This procedure is based on a direct relationship between gravity disturbances at flight level and the disturbing gravity potential at sea level. This procedure provided the best results in terms of accuracy, stability and numerical efficiency. As a general result, numerically stable downward continuation of airborne gravity data can be seen as another advantage of airborne gravimetry in the field of geoid determination.

Keywords: Downward continuation – Airborne Gravimetry – Geoid – Band-limited Gravity

Correspondence to: P. Novák,
Geodetic Observatory Pecny, 251 65 Ondrejov 244,
Czech Republic.
e-mail: pnovak@pecny.asu.cas.cz; Tel.: +420 204 649 235;
Fax: +420 204 649 236

1 Introduction

Airborne gravity data, observed by airborne gravimeters or derived from a combined evaluation of signals observed by INS (inertial navigation system) sensors and GPS (global positioning system) receivers, can easily be transformed into gravity disturbances at flight level. A principal aim of airborne gravity field determination is the derivation of the disturbing gravity potential or geoidal undulations at ground or mean sea level. This can be achieved by first calculating the disturbing gravity potential at flight level from the observed gravity disturbances, and then downward continuing the disturbing gravity potential from flight level to sea level. In recent years the procedure, based on inverting the solution of Dirichlet's problem of potential theory, has become a standard technique applied by many authors (e.g. Huestis and Parker 1979; Vaníček et al. 1996; Martinec 1998; Sjöberg 2001).

Due to the noisy nature of airborne observations of gravity, caused by flight dynamics, the recorded gravity signal must be low-pass filtered, which results in recovery of low-frequency gravity information. Since the reference gravity, computed from available global geopotential models (GGMs), is subtracted from observed gravity, airborne gravimetry provides only discrete samples of band-limited gravity. This band limitation has a positive impact on the downward continuation in stabilizing significantly its numerical evaluation. Two different approaches for the harmonic downward continuation of the band-limited disturbing gravity potential are formulated in this contribution. The first approach, commonly used also for the harmonic downward continuation of ground gravity data to sea level, is based on the inverse of Abel–Poisson's integral, resulting in a Fredholm integral equation of the first kind. In contrast, the idea behind the second approach is to avoid numerically unstable inverse solutions by setting up a direct relationship between gravity potentials at flight level and sea level. While the

former approach can be used for any vertical distribution of data, the latter method can only be applied to data distributed over flight level with almost constant height above the reference ellipsoid. This restriction does not allow for a general use of the latter model and its applicability is thus limited to airborne data.

Both these approaches rely on a two-step procedure involving two steps of integration. As an alternative, a one-step procedure can be constructed, based on a transformation of band-limited gravity disturbances at flight level directly into the disturbing gravity potential at sea level. In this approach, the transformations of gravity disturbances into the disturbing gravity potential (smoothing step) and the downward continuation (roughening step) are fused. As a result, an improved numerical behaviour and better stability of the solution can be expected.

The three approaches are described in detail in Sect. 2. Since airborne gravity data are available over local regions only, spherical cap integration is applied, calculating truncation errors approximately on the basis of an available GGM in terms of spherical harmonics. All three approaches are tested for accuracy, efficiency and stability using noisy synthetic airborne gravity data in Sect. 3. The results are discussed in Sect. 4, where conclusions of the presented research are also drawn.

2 Theory

Assuming that the band-limited gravity disturbances δg^b , derived from airborne gravimetry, are given at constant flight level, the problem is to determine the band-limited disturbing gravity potential T^b , harmonic outside the geocentric reference sphere of radius R (spherical approximation of the geoid). Formally, this is no longer a boundary-value problem but rather an initial-value problem, since the data are given in the solution domain itself and not on the boundary. Related to the Stokesian approach for the determination of the geoid, this type of problem has been called a pseudo-boundary-value problem (Sansò 1995). In the spherical approximation, the following formulation can be given to this problem:

$$\begin{aligned} \nabla^2 T^b(r, \Omega) &= 0 \quad \text{for } r > R \\ \delta g^b(r, \Omega) &= -\left. \frac{\partial T^b(r, \Omega)}{\partial r} \right|_r \quad \text{for } r = R + H \\ T^b(r, \Omega) &= \mathcal{O}(r^{-\ell-1}) \quad \text{for } r \rightarrow \infty \end{aligned} \quad (1)$$

\mathcal{O} stands for the Landau symbol, (r, Ω) for the spherical coordinate triad, and ℓ is the minimum degree of the band-limited gravity disturbances δg^b . H is a known constant height of the flight trajectory above mean sea level. Although the solution to the initial-value problem of Eqs. (1), if it exists and is unique, is unstable in general, the property of band-limited data, given on a smooth surface, transfers the originally improperly posed problem to a properly posed one (e.g. Martinec 1998).

In the following, three alternatives for the solution of the initial-value problem of Eqs. (1) are considered. The

first and the second approaches are based on a two-step procedure, involving as a first step the transformation of band-limited airborne gravity disturbances δg^b , reduced for effects of topographical and atmospheric masses, into the band-limited disturbing gravity potential T^b at flight level using the spherical Hotine integral

$$T^b(R + H, \Omega) = \frac{R + H}{4\pi} \iint_{\Theta} \delta g^b(R + H, \Omega') \mathcal{H}^b(\psi) d\Omega' \quad (2)$$

where Θ is the full spatial angle. \mathcal{H}^b is the band-limited spherical Hotine function (Novák et al. 2001)

$$\mathcal{H}^b(\psi) = \sum_{n=\ell}^{\ell+b} \frac{2n+1}{n+1} P_n(\cos \psi) \quad (3)$$

P_n stands for the Legendre polynomials (Heiskanen and Moritz 1967). The spherical distance ψ between geocentric directions $\Omega = (\varphi, \lambda)$ and $\Omega' = (\varphi', \lambda')$ can be computed by spherical trigonometry

$$\cos \psi = \cos \varphi \cos \varphi' + \sin \varphi \sin \varphi' \cos(\lambda - \lambda') \quad (4)$$

The second step then consists of the downward continuation of the harmonic function T^b from flight level to sea level, which is again approximated by the reference sphere. Two proposals for the downward continuation of the band-limited disturbing gravity potential T^b are studied. While the first approach is based on solving an inverse problem, a direct approach is used in the second procedure.

In contrast, the third approach, presented in Sect. 2.3, relies on a one-step procedure, transforming the band-limited airborne gravity disturbances δg^b at flight level directly into the band-limited disturbing gravity potential T^b at sea level. It should be noticed that the applicability of the three approaches is clearly limited to airborne gravity data due to the assumption that the airborne gravity disturbances δg^b are observed at constant height H .

2.1 Two-step approach: downward continuation as an inverse problem

The harmonic band-limited disturbing gravity potential T^b can be expanded on the surface of the reference sphere as follows:

$$T^b(R, \Omega) = \frac{GM}{R} \sum_{n=\ell}^{\ell+b} T_n(\Omega) \quad (5)$$

where T_n are the Laplace spherical harmonics and GM denotes the geocentric gravitational constant. The minimum frequency of the harmonic band-limited disturbing gravity potential T^b and gravity disturbances δg^b is characterized in the following by the degree ℓ and their maximum frequency by $\ell + b$. Current values for airborne data are $\ell \leq 361$ and approximately $\ell + b \leq 2200$, respectively. The upward continuation of T^b from the reference sphere of radius R into external space can be solved using the spherical Dirichlet problem, which reads

$$\begin{aligned} \nabla^2 T^b(r, \Omega) &= 0 \quad \text{for } r > R \\ T^b(r, \Omega) &= f(r, \Omega) \quad \text{for } r = R \\ T^b(r, \Omega) &= \mathcal{O}(r^{-\ell-1}) \quad \text{for } r \rightarrow \infty \end{aligned} \quad (6)$$

It is assumed that the function f , i.e. the band-limited disturbing gravity potential, is known on the reference sphere as a result of the first step. The solution to the problem of Eqs. (6) for T^b at flight level $R + H$ in terms of the Green function is represented by the Abel–Poisson integral (Kellogg 1929)

$$T^b(R + H, \Omega) = \frac{1}{4\pi} \iint_{\Theta} T^b(R, \Omega') \mathcal{P}^b(R, \psi, R + H) d\Omega' \quad \text{for } H \geq 0 \quad (7)$$

The band-limited spherical Abel–Poisson function is of the form

$$\mathcal{P}^b(R, \psi, R + H) = \sum_{n=\ell}^{\ell+b} (2n+1) \left(\frac{R}{R+H} \right)^{n+1} P_n(\cos \psi) \quad (8)$$

The solution for T^b at sea level (approximated in the solution by the reference sphere of radius R) can be found using the inversion of Eq. (7) for known values of T^b at flight level $R + H$. Equation (7) thus turns into a Fredholm integral equation of the first kind. The global integration over the full spatial angle Θ in Eq. (7) cannot, however, be carried out in the global sense due to the lack of observed data. For practical computations, Eq. (7) can only be approximated, applying integration over a spherical cap around the computation point and calculating the truncation errors by the aid of the GGM. For example, a simple numerical integration yields for the computation point Ω_i

$$\begin{aligned} T^b(R + H, \Omega_i) - \frac{GM}{2R} \sum_{n=\ell}^L D_n(H, \psi_o) T_n(\Omega_i) \\ = \frac{1}{4\pi} \sum_{j=1}^N T^b(R, \Omega_j) \mathcal{P}^b(R, \psi_{ij}, R + H) \Delta\Omega_j, \end{aligned} \quad L \leq \ell + b \quad (9)$$

Here, $\Delta\Omega_j$ is the area of the trapezoidal cell centered at the j th geographical node Ω_j , N is the number of data within the spherical cap of radius ψ_o , and T_n are the Laplace harmonics of the disturbing gravity potential derived, for example, from the EGM96 (Lemoine et al. 1998) of maximum degree L . The truncation coefficients D_n of the band-limited Abel–Poisson function are (Molodenskij et al. 1960)

$$D_n(H, \psi_o) = \sum_{m=\ell}^{\ell+b} (2m+1) \left(\frac{R}{R+H} \right)^{m+1} R_{n,m}(\psi_o), \quad \ell \leq n \leq L \quad (10)$$

Numerical values of the truncation coefficients D_n for $H = 4$ km and $\psi_o = 1^\circ$ are plotted in Fig. 1. Coefficients $R_{n,m}$

$$R_{n,m}(\psi_o) = \int_{\psi=\psi_o}^{\pi} P_n(\cos \psi) P_m(\cos \psi) \sin \psi d\psi \quad (11)$$

can conveniently be computed by an iterative expression [Paul 1973, Eq. (5)].

The matrix form of Eq. (9) reads

$$\mathbf{T}^b(\mathbf{R} + \mathbf{H}) = \frac{1}{4\pi} \mathbf{A} \mathbf{T}^b(\mathbf{R}) \quad (12)$$

where the known vector $\mathbf{T}^b(\mathbf{R} + \mathbf{H})$ is reduced by the effect of the data outside the spherical cap given by the spherical harmonic series on the left-hand side of Eq. (9). The off-diagonal entries of the matrix \mathbf{A} are given as follows (Martinec 1998):

$$A_{ij} = \begin{cases} \mathcal{P}^b(R, \psi_{ij}, R + H) \Delta\Omega_j & \text{for } \psi_{ij} \leq \psi_o \\ 0 & \text{for } \psi_{ij} > \psi_o \end{cases} \quad (13)$$

The diagonal entries in the matrix \mathbf{A} are given for N gravity data within the spherical cap of radius ψ_o as follows:

$$\begin{aligned} A_{ii} &= 2\pi \int_{\psi=0}^{\psi_o} \mathcal{P}^b(R, \psi, R + H) \sin \psi d\psi \\ &\quad - \sum_{j=1, j \neq i}^N \mathcal{P}^b(R, \psi_{ij}, R + H) \Delta\Omega_j \end{aligned} \quad (14)$$

The integral of the modified band-limited Poisson function can be evaluated as follows:

$$\begin{aligned} \int_{\psi=0}^{\psi_o} \mathcal{P}^b(R, \psi, R + H) \sin \psi d\psi \\ = - \sum_{n=\ell}^{\ell+b} (2n+1) \left(\frac{R}{R+H} \right)^{n+1} R_n(\psi_o) \end{aligned} \quad (15)$$

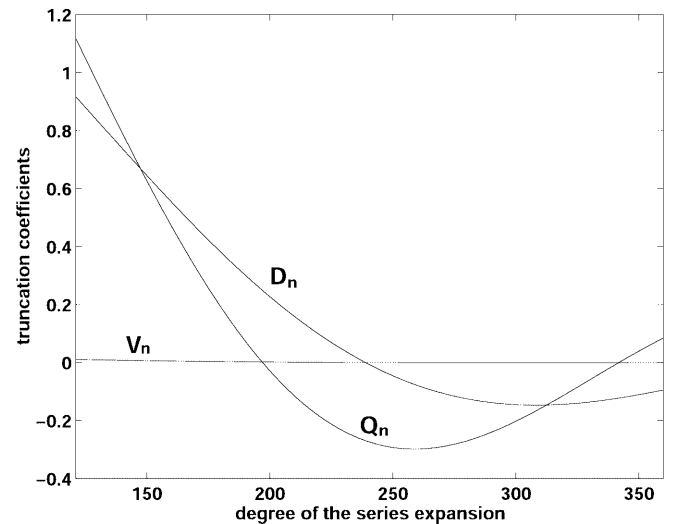


Fig. 1. Truncation coefficients D_n , Q_n and V_n for $\psi_o = 1^\circ$ and $H = 4$ km

where R_n represents the analytical solution to the integral of the Legendre function (Paul 1973)

$$R_n(\psi_o) = - \int_{\psi=0}^{\psi_o} P_n(\cos \psi) \sin \psi \, d\psi$$

$$= \frac{P_{n+1}(\cos \psi_o) - P_{n-1}(\cos \psi_o)}{2n+1} \quad (16)$$

The truncation errors for $\psi_o = 1^\circ$ induced by neglecting the outer zone of integration (see Fig. 2) refer to the numerical example treated in Sect. 3. The system of linear equations, Eq. (12), for the column vector $\mathbf{T}^b(\mathbf{R})$ is uniquely solvable only if \mathbf{A} is a square matrix, i.e. if the dimension of $\mathbf{T}^b(\mathbf{R})$ and $\mathbf{T}^b(\mathbf{R} + \mathbf{H})$ is identical. The solution of Eq. (12) can be complicated by a possibly ill-conditioned matrix operator \mathbf{A} . Moreover, small variations in $\mathbf{T}^b(\mathbf{R} + \mathbf{H})$ (such as observation errors) can cause large and unrealistic variations in calculated $\mathbf{T}^b(\mathbf{R})$. In other words, the solution can be numerically unstable and regularization of the model (smoothing) may be the only alternative to arrive at some reasonable solution.

2.2 Two-step approach: direct approach to downward continuation

Airborne gravimetry provides gravity data collected at flight level of almost constant height which can easily be approximated by a geocentric sphere of radius $R + H$. A spherical initial-value problem can alternatively be formulated for the flight level as the boundary, after having transformed the gravity disturbances $\delta g^b(R + H, \Omega)$ into the disturbing gravity potential $T^b(R + H, \Omega)$ in the first step [see Eq. (2)]. The spherical approximation can be used in this case due to relatively small vertical deviations of observation points from mean height H (deviations at the level of few metres are observed for actual airborne data). This initial-value problem can be written as follows:

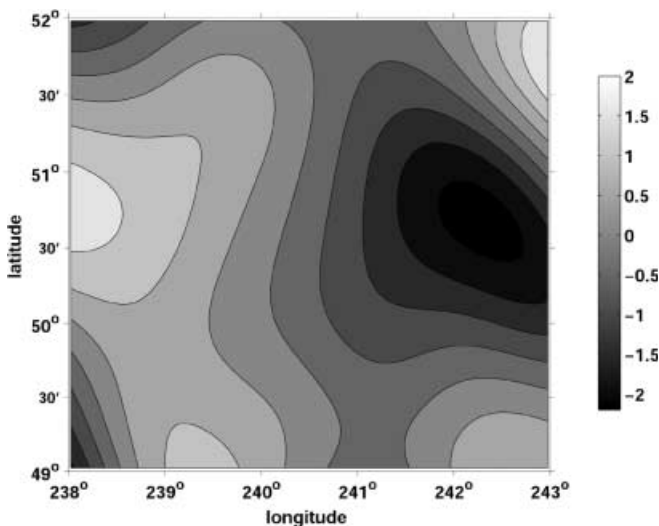


Fig. 2. Truncation errors in the inverse two-step approach ($\text{m}^2 \text{s}^{-2}$)

$$\nabla^2 T^b(r, \Omega) = 0 \quad \text{for } r > R$$

$$T^b(r, \Omega) = f(r, \Omega) \quad \text{for } r = R + H \quad (17)$$

$$T^b(r, \Omega) = \mathcal{O}(r^{-\ell-1}) \quad \text{for } r \rightarrow \infty$$

Values of the function f can be derived from airborne gravity disturbances at flight level $R + H$ using the spherical Hotine integral [see Eq. (2)]. The solution to the initial-value problem of Eqs. (17) can be written as follows:

$$T^b(R, \Omega) = \frac{1}{4\pi} \iint_{\Theta} T^b(R + H, \Omega') \mathcal{K}^b(R, \psi, R + H) \, d\Omega'$$

for $H \geq 0$ (18)

The band-limited integration kernel \mathcal{K}^b is of the form

$$\mathcal{K}^b(R, \psi, R + H) = \sum_{n=\ell}^{\ell+b} (2n+1) \left(\frac{R+H}{R}\right)^{n+1} P_n(\cos \psi) \quad (19)$$

The solution of Eq. (18) can obviously be used for certain fixed values of parameters b and H only. In the case of actual airborne data, approximate maximum values of 6 km for H and 4000 for $\ell + b$ can be expected (for minimum data resolution of 4–5 km full wavelength expected for future gravity data). Both values would guarantee stable numerical evaluation of the integral of Eq. (18). The function \mathcal{K}^b for $\ell = 121$ and $\ell + b = 4320$ (resolution of 2.5 arcmin) is plotted in Fig. 3. The upper graph (the function \mathcal{K}^b by degree n at $\psi = 1^\circ$) shows clearly the divergent nature of the function for $\ell + b \rightarrow \infty$. The divergence rate is higher with increasing elevation H . The lower graph of the same figure shows the kernel \mathcal{K}^b as a function of the spherical distance ψ for $\ell = 121$ and $\ell + b = 4320$.

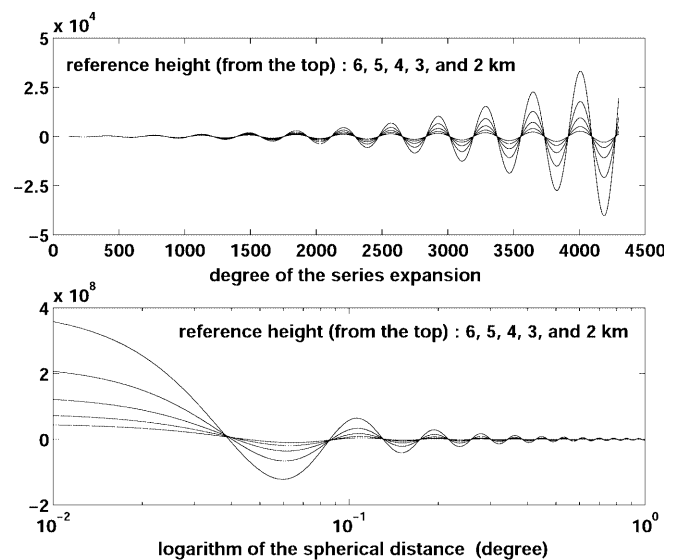


Fig. 3. Band-limited integration kernel \mathcal{K}^b for $121 \leq n \leq 4320$. **Upper graph:** kernel by degree n at $\psi = 1^\circ$; **lower graph:** kernel as a function of ψ

Applying the simple integration, the integral of Eq. (18) is of the form

$$\begin{aligned} T^b(R, \Omega_i) - \frac{GM}{2R} \sum_{n=\ell}^L \left(\frac{R}{R+H} \right)^{n+1} Q_n(H, \psi_o) T_n(\Omega_i) \\ = \frac{1}{4\pi} \sum_{j=1}^N T^b(R+H, \Omega_j) \mathcal{K}^b(R, \psi_{ij}, R+H) \Delta\Omega_j, \end{aligned} \quad L \leq \ell + b \quad (20)$$

Truncation coefficients Q_n of the function \mathcal{K}^b are

$$Q_n(H, \psi_o) = \sum_{m=\ell}^{\ell+b} (2m+1) \left(\frac{R+H}{R} \right)^{m+1} R_{n,m}(\psi_o), \quad \ell \leq n \leq L \quad (21)$$

Numerical values of the truncation coefficients Q_n for $H = 4$ km and $\psi_o = 1^\circ$ are also plotted in Fig. 1. The truncation coefficients D_n and Q_n can be compared in this figure. The larger numerical values of the coefficients Q_n would mean larger truncation errors. Since the coefficients Q_n are multiplied by the attenuation factor to the power of $n+1$, the truncation errors have comparable magnitude in both the inverse and direct approaches (see Figs. 2 and 4). The truncation errors can be decreased further by suitable modification of the integration kernel.

The matrix form of Eq. (20) can be written concisely as

$$\mathbf{T}^b(\mathbf{R}) = \frac{1}{4\pi} \mathbf{B} \mathbf{T}^b(\mathbf{R} + \mathbf{H}) \quad (22)$$

where the unknown vector $\mathbf{T}^b(\mathbf{R})$ is reduced by the contribution of the corresponding remote-zone data (see Fig. 4) given by the spherical harmonic series on the left-hand side of Eq. (20). These values also refer to the numerical example in Sect. 3. The off-diagonal entries of the matrix \mathbf{B} are given as follows:

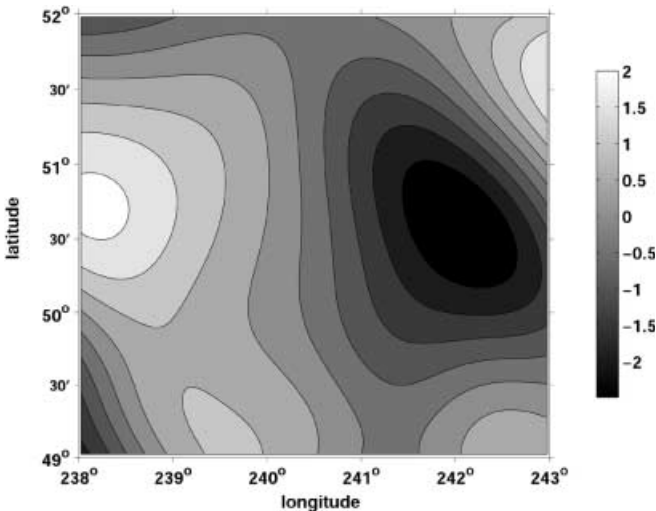


Fig. 4. Truncation errors in the direct two-step approach ($\text{m}^2 \text{s}^{-2}$)

$$B_{ij} = \begin{cases} \mathcal{K}^b(R, \psi_{ij}, R+H) \Delta\Omega_j & \text{for } \psi_{ij} \leq \psi_o \\ 0 & \text{for } \psi_{ij} > \psi_o \end{cases} \quad (23)$$

The diagonal entries in the matrix \mathbf{B} are given for N gravity data within the spherical cap of radius ψ_o as follows:

$$\begin{aligned} B_{ii} = 2\pi \int_{\psi=0}^{\psi_o} \mathcal{K}^b(R, \psi, R+H) \sin \psi \, d\psi \\ - \sum_{j=1, j \neq i}^N \mathcal{K}^b(R, \psi_{ij}, R+H) \Delta\Omega_j \end{aligned} \quad (24)$$

The integral of the modified band-limited function \mathcal{K}^b can be evaluated as follows:

$$\begin{aligned} \int_{\psi=0}^{\psi_o} \mathcal{K}^b(R, \psi, R+H) \sin \psi \, d\psi \\ = - \sum_{n=\ell}^{\ell+b} (2n+1) \left(\frac{R+H}{R} \right)^{n+1} R_n(\psi_o) \end{aligned} \quad (25)$$

with the function R_n already defined in Eq. (16). Since no inverse is involved in Eq. (22), no instabilities are expected in the numerical evaluation of this system of linear equations. In contrast to the approach described in Sect. 2.1, the number of unknowns and data points may be different.

2.3 One-step approach: transformation of the gravity disturbances at flight level to the disturbing gravity potential at sea level

Instead of the two-step procedure, presented above in Sects. 2.1 and 2.2, a direct solution of the pseudo-boundary-value problem of Eqs. (1) for the band-limited disturbing gravity potential T^b can be derived. This procedure results in the following solution formula for the band-limited gravity disturbances δg^b at flight level, derived from airborne gravimetry:

$$\begin{aligned} T^b(R, \Omega) = \frac{R+H}{4\pi} \iint_{\Theta} \delta g^b(R+H, \Omega') \\ \times \mathcal{J}^b(R, \psi, R+H) d\Omega' \quad \text{for } H \geq 0 \end{aligned} \quad (26)$$

The band-limited integration kernel \mathcal{J}^b reads

$$\mathcal{J}^b(R, \psi, R+H) = \sum_{n=\ell}^{\ell+b} \frac{2n+1}{n+1} \left(\frac{R+H}{R} \right)^{n+1} P_n(\cos \psi) \quad (27)$$

The kernel function \mathcal{J}^b for $\ell = 121$ and $\ell + b = 4320$, and five different flight heights H is plotted in Fig. 5. A comparison with Fig. 3 proves that – due to the smaller absolute variations – the kernel \mathcal{J}^b related to the one-step procedure is numerically much more stable than the kernel \mathcal{K}^b related to the direct two-step procedure even for higher flight levels.

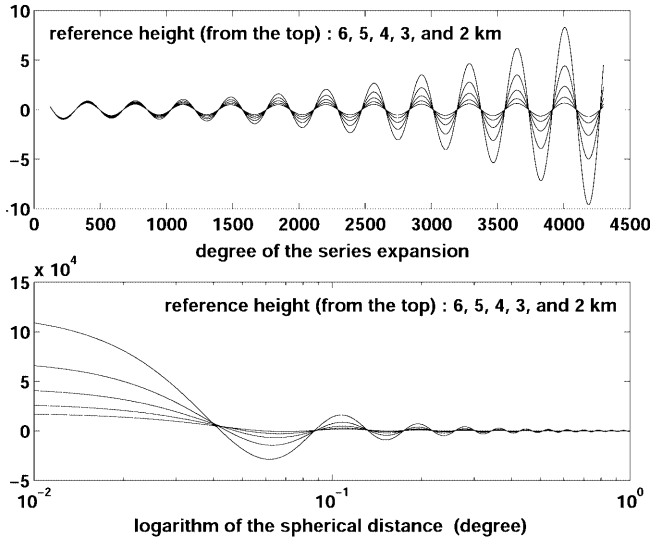


Fig. 5. Band-limited integration kernel \mathcal{J}^b for $121 \leq n \leq 4320$. **Upper graph:** kernel by degree n at $\psi = 1^\circ$; **lower graph:** kernel as a function of ψ

Applying the simple integration and considering the truncation error resulting from spherical cap integration, the discretized integral of Eq. (26) takes the form

$$\begin{aligned} T^b(R, \Omega_i) - \frac{GM}{2(R+H)} \sum_{n=\ell}^L (n+1) \left(\frac{R}{R+H} \right)^{n+1} \\ \times V_n(H, \psi_o) T_n(\Omega_i) \\ = \frac{R+H}{4\pi} \sum_{j=1}^N \delta g^b(R+H, \Omega_j) \mathcal{J}^b(R, \psi_{ij}, R+H) \Delta\Omega_j, \quad L \leq \ell + b \end{aligned} \quad (28)$$

The truncation coefficients V_n of the function \mathcal{J}^b are

$$V_n(H, \psi_o) = \sum_{m=\ell}^{\ell+b} \frac{2m+1}{m+1} \left(\frac{R+H}{R} \right)^{m+1} R_{n,m}(\psi_o), \quad \ell \leq n \leq L \quad (29)$$

Numerical values of the truncation coefficients V_n for $H = 4$ km and $\psi_o = 1^\circ$ are plotted in Fig. 1. A comparison in Fig. 1 shows that the coefficients V_n are several orders of magnitude smaller than the truncation coefficients D_n and Q_n . The numerical values of the coefficients V_n also change only slightly within the range of flight heights used. The truncation errors presented in Fig. 6 also refer to the example in Sect. 3. They could be decreased by modification of the integration kernel.

The matrix form of Eq. (28) can be written concisely as

$$\mathbf{T}^b(\mathbf{R}) = \frac{R+H}{4\pi} \mathbf{C} \delta \mathbf{g}^b(\mathbf{R} + \mathbf{H}) \quad (30)$$

where the unknown vector $\mathbf{T}^b(\mathbf{R})$ is reduced by the contribution of the corresponding remote-zone data given by the spherical harmonic series on the left-hand

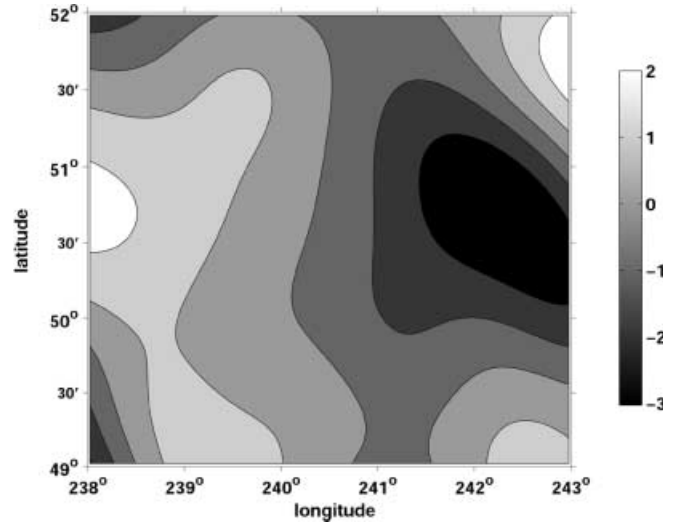


Fig. 6. Truncation errors in the one-step approach ($\text{m}^2 \text{s}^{-2}$)

side of Eq. (28). The off-diagonal entries of the matrix \mathbf{C} are given as follows:

$$C_{ij} = \begin{cases} \mathcal{J}^b(R, \psi_{ij}, R+H) \Delta\Omega_j & \text{for } \psi_{ij} \leq \psi_o \\ 0 & \text{for } \psi_{ij} > \psi_o \end{cases} \quad (31)$$

The diagonal entries in the matrix \mathbf{C} read for N gravity data within the spherical cap of radius ψ_o

$$\begin{aligned} C_{ii} = 2\pi \int_{\psi=0}^{\psi_o} \mathcal{J}^b(R, \psi, R+H) \sin \psi \, d\psi \\ - \sum_{j=1, j \neq i}^N \mathcal{J}^b(R, \psi_{ij}, R+H) \Delta\Omega_j \end{aligned} \quad (32)$$

The integral of the modified band-limited function \mathcal{J}^b can be evaluated as follows:

$$\begin{aligned} \int_{\psi=0}^{\psi_o} \mathcal{J}^b(R, \psi, R+H) \sin \psi \, d\psi \\ = - \sum_{n=\ell}^{\ell+b} \frac{2n+1}{n+1} \left(\frac{R+H}{R} \right)^{n+1} R_n(\psi_o) \end{aligned} \quad (33)$$

with the function R_n already defined in Eq. (16). Again no inverse is involved in Eq. (30), so no instabilities are expected in the numerical evaluation of these relationships. Also in this approach – in contrast to the approach in Sect. 2.1 – the number of unknowns and data points may be different.

3 Numerical tests

In order to test numerical accuracy, efficiency and stability of all three approaches that were described in the previous section, a synthetic GGM (SGM) was used

for computation of the band-limited gravity disturbances at flight level $R + H$

$$\delta g^b(R + H, \Omega) = \frac{GM}{R^2} \sum_{n=\ell}^{\ell+b} (n+1) \left(\frac{R}{R+H} \right)^{n+2} T_n(\Omega) \quad (34)$$

Values of $\ell = 121$ and $\ell + b = 2160$ were used with respect to spectral content of current airborne gravity data. Higher-degree coefficients T_n of the SGM were adjusted (Novák et al. 2001) in order to fit the GPM98 degree variances (Wenzel 1998) (see Fig. 7) derived from actual gravity data. Five different flight levels, with heights H of 2, 3, 4, 5 and 6 km, were used as typical values expected for actual airborne data. The test area was limited by two parallels of 49° and 52° northern latitude, and by two meridians of 238° and 243° eastern longitude. This area corresponds to 8640 data points spaced by 2.5 arcmin in latitude and longitude. Due to the integration radius $\psi_o = 1^\circ$ used in the Abel–Poisson integration, the computation area was bounded by latitude of 50° and 51° and by longitude of 240° and 241° in order to avoid any edge effects in the results. This corresponds to 576 computation points spaced by 2.5 arcmin in latitude and longitude.

The scheme of the numerical tests is shown in Fig. 8. The random noise $\varepsilon^g(R + H)$ of 1.5 mGal was added first to the values of gravity disturbances δg^b at flight level generated from the SGM by Eq. (34). The gravity noise ε^g is shown in Fig. 9. In the two-step approaches, the band-limited disturbing gravity potential T^b at flight level was first derived from noisy gravity disturbances using the spherical Hotine formula (HTN) [see Eq. (2)]. The random noise $\varepsilon^g(R + H)$ of 1.5 mGal added to the gravity disturbances propagated via the Hotine integral formula into the noise $\varepsilon^T(R + H)$ of approximately $0.05 \text{ m}^2 \text{ s}^{-2}$. These values were obtained by comparing the results of the Hotine integration with the reference values generated directly from the SGM

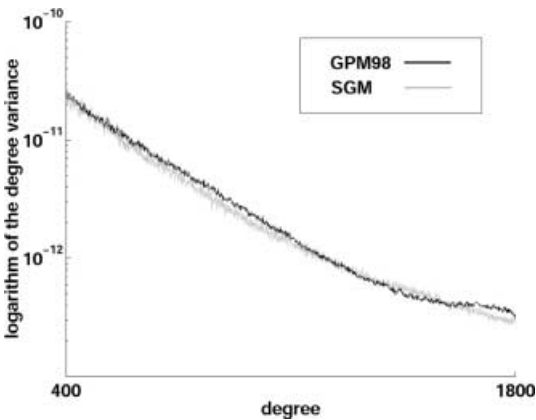


Fig. 7. GPM98b versus SGM degree variances of degree 400–1800 (mGal^2)

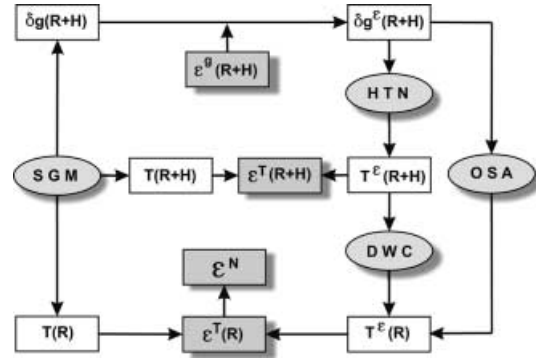


Fig. 8. Scheme for testing the solution alternatives

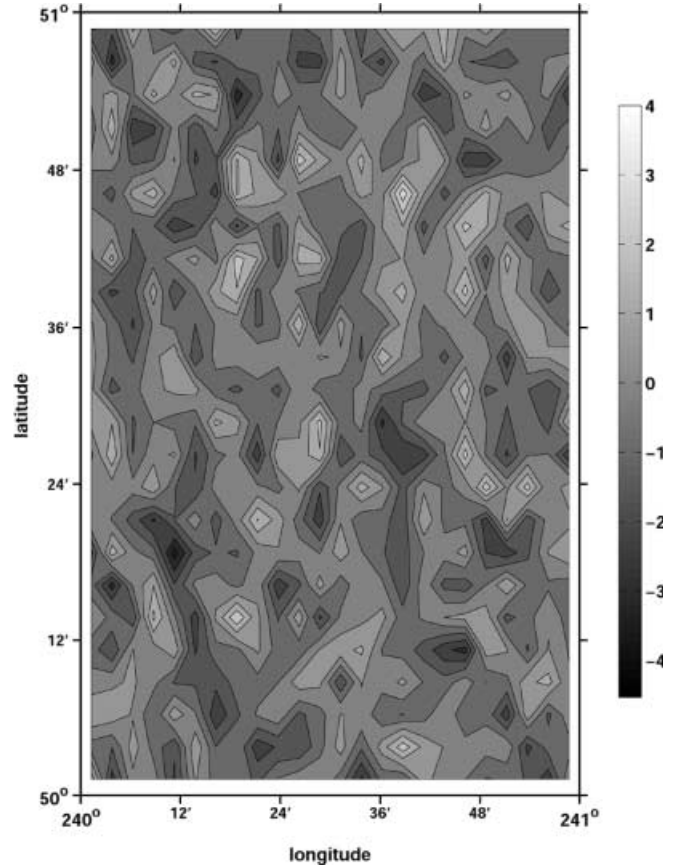


Fig. 9. Gravity noise ε^g added to the synthetic airborne data (mGal)

$$T^b(R + H, \Omega) = \frac{GM}{R} \sum_{n=\ell}^{\ell+b} \left(\frac{R}{R+H} \right)^{n+1} T_n(\Omega) \quad (35)$$

The Hotine integral, being a low-pass filter, effectively reduced high-frequency noise in the gravity data, which had positive consequences for the downward continuation step (DWC) following next in the two-step approaches. The noisy band-limited disturbing gravity potential T^b was downward continued from flight level $R + H$ to sea level (approximated again by the reference sphere of radius R) using either the inverse or the direct approach. In the one-step approach (OSA), the noisy gravity disturbances δg^b at flight level were

transformed directly into the noisy band-limited disturbing gravity potential T^b at sea level. Results of the three approaches were compared against reference values computed directly from the SGM by the series expansion

$$T^b(R, \Omega) = \frac{GM}{R} \sum_{n=\ell}^{\ell+b} T_n(\Omega) \quad (36)$$

The differences, used for evaluation of the noise propagation, were converted into the effect on the geoid using the Bruns formula in spherical approximation (Heiskanen and Moritz 1967)

$$\varepsilon^N = \frac{\varepsilon^T(R)}{\gamma} \quad (37)$$

with normal gravity γ . Results for the two-step approach with the inverse downward continuation are tabulated in Table 1, for the two-step approach with the direct downward continuation in Table 2, and for the one-step approach in Table 3, for different flight levels.

The results for the two-step approach with the inverse downward continuation (see Table 1) show all the well-known signs of numerical instability. Clearly, the noise magnification for flying altitudes above 4 km makes the results unusable for accurate geoid determination. In the worst case, the initial random noise in gravity disturbances of 1.5 mGal propagates via the Hotine and inverse Abel–Poisson integral into geoid noise of 25 cm. The bias stays negligibly small for all solutions. The noise ε^N in the geoidal undulations obtained using this

Table 1. Geoid noise ε^N for the inverse two-step approach (m)

Height (km)	Minimum	Maximum	Mean	Sigma	RMS
2	-0.026	+0.034	+0.001	± 0.010	± 0.010
3	-0.053	+0.060	+0.001	± 0.019	± 0.019
4	-0.120	+0.121	+0.002	± 0.045	± 0.045
5	-0.323	+0.315	+0.002	± 0.112	± 0.112
6	-0.748	+0.709	+0.002	± 0.252	± 0.252

Table 2. Geoid noise ε^N for the direct two-step approach (m)

Height (km)	Minimum	Maximum	Mean	Sigma	RMS
2	-0.014	+0.027	+0.005	± 0.009	± 0.010
3	-0.019	+0.033	+0.006	± 0.010	± 0.012
4	-0.024	+0.041	+0.008	± 0.013	± 0.015
5	-0.031	+0.052	+0.010	± 0.017	± 0.019
6	-0.041	+0.066	+0.013	± 0.021	± 0.025

Table 3. Geoid noise ε^N for the one-step approach (m)

Height (km)	Minimum	Maximum	Mean	Sigma	RMS
2	-0.017	+0.022	+0.005	± 0.008	± 0.010
3	-0.017	+0.023	+0.006	± 0.008	± 0.010
4	-0.020	+0.025	+0.006	± 0.009	± 0.010
5	-0.024	+0.027	+0.006	± 0.010	± 0.011
6	-0.029	+0.031	+0.006	± 0.011	± 0.013

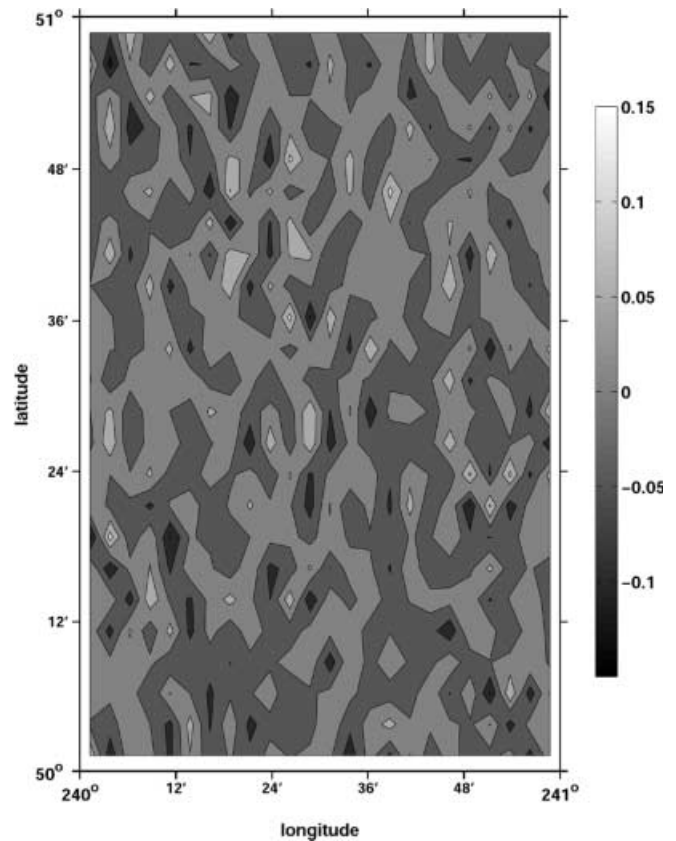


Fig. 10. Geoid noise ε^N from the inverse two-step approach (m)

approach for the airborne data at a flight height of 4 km is shown in Fig. 10.

The results for the two-step approach with the direct downward continuation (see Table 2) have quite different characteristics. The noise magnification associated with the inverse approach cannot be observed in the results obtained by this approach. The noise level increases very slightly with increasing flight height H . The noise magnification is one order of magnitude smaller for the maximum flight height of 6 km when the results of the inverse and direct approaches are compared. There is a bias present in all solutions from the direct approach which can reach values of 1 cm. The noise ε^N in the geoidal undulations obtained using this approach for the airborne data at a flight height of 4 km is shown in Fig. 11.

The results for the one-step approach (see Table 3), are even more accurate than those for the previous approach. However, this approach also has some additional advantages. It is numerically much more efficient, requiring only one integration step for the computation of the solution. The ratio of flight height to resolution, so critical for the inverse downward continuation, can be avoided. Moreover, the data area usually required for a solution unaffected by the edge effects can be smaller in this case. This solution represents an elegant solution to the problem of the geoid determination from airborne gravity and gives the airborne gravimetry a significant advantage compared

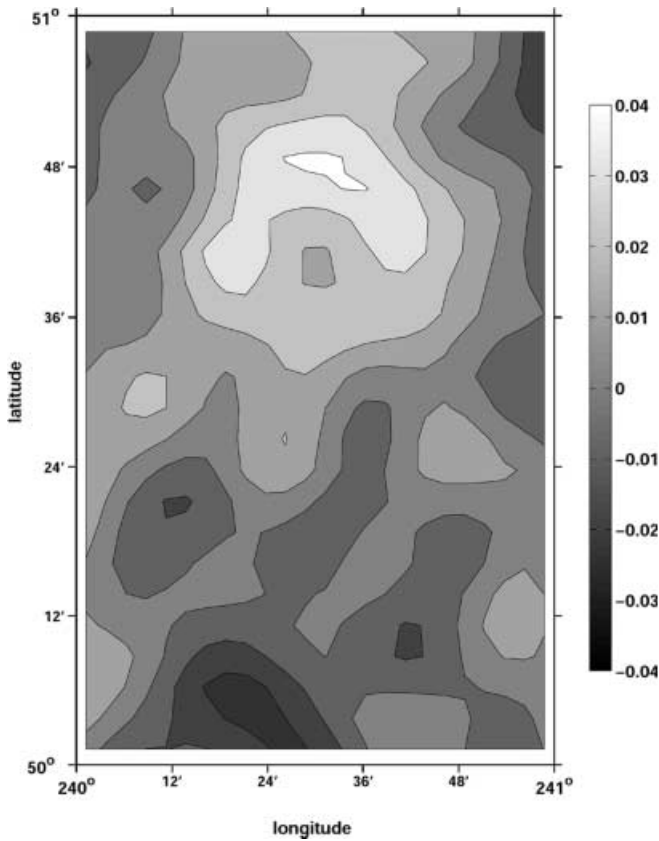


Fig. 11. Geoid noise ε^N from the direct two-step approach (m)

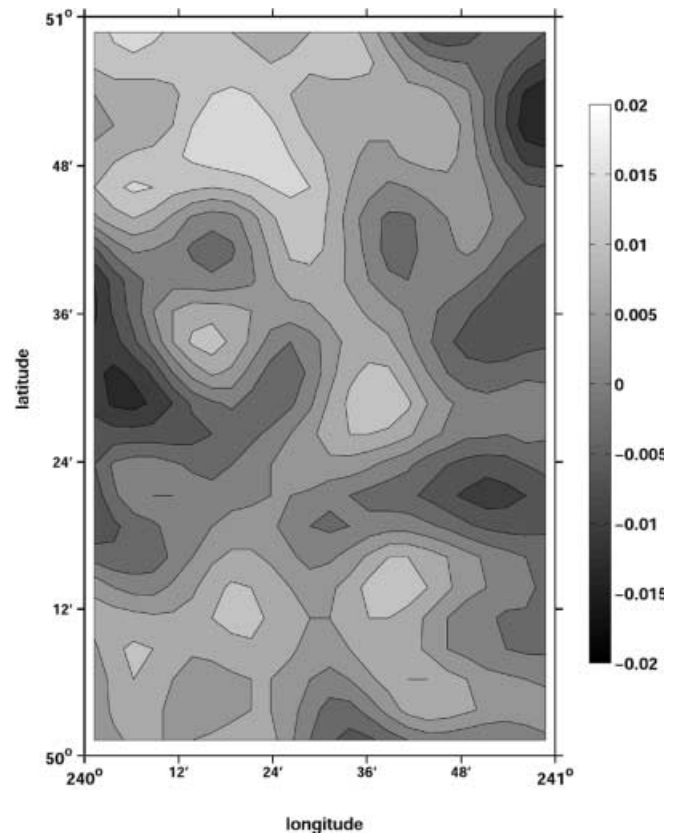


Fig. 12. Geoid noise ε^N from the one-step approach (m)

to ground gravity data. The noise ε^N in the geoidal undulations obtained using the one-step approach for the airborne data at flight height of 4 km is shown in Fig. 12. All three approaches can finally be compared in terms of the noise propagation (standard deviation) that is plotted in Fig. 13.

4 Conclusions

The determination of the disturbing gravity potential and geoidal heights at mean sea level from band-limited airborne gravity data at flight level has been discussed. Simulated gravity data, generated from the high-frequency SGM and distorted by the random noise expected for actual airborne data, were used for numerical testing of the three solution alternatives. Although they should provide the same results from the analytical point of view, there are significant differences in the results due to the propagation of observation errors and truncation errors.

The first and the second approaches are based on a two-step procedure, the first step consisting of the determination of the disturbing gravity potential from gravity disturbances at flight level, while in the second step the downward continuation to mean sea level is considered. The first approach, based on the inverse of the Abel–Poisson integral, provided numerically unstable results with unreasonably large noise magnification. These results could be expected. Additional

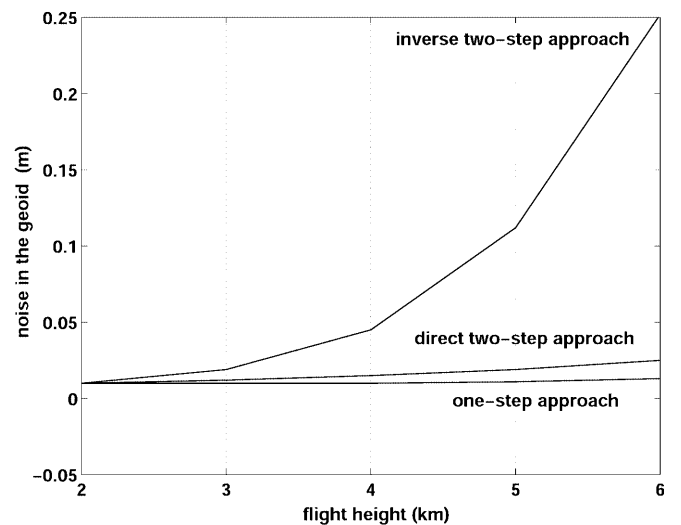


Fig. 13. Geoid noise ε^N from the three approaches as a function of flight height (m)

modifications of the procedure, e.g. by the Tikhonov regularization, would have to be applied in order to arrive at more reasonable results. The second approach, using a direct solution of the respective initial-value problem for band-limited data, can provide stable solutions without any further regularization. The results obtained for high-frequency synthetic data did not show any of the numerical instabilities present in

the inverse solutions. The bias of the results in the direct model was somewhat larger compared to that of the inverse model. However, it stayed within the noise level of the results and its impact on the geoid reached about 1 cm. Although the direct approach does not solve the problem of downward continuation of gravity data distributed at different heights, it can be used successfully for band-limited airborne data, avoiding in this way numerically unstable inverse solutions.

The third solution approach is based on a one-step procedure, making use of the direct relationship between gravity disturbances at flight level and the disturbing gravity potential at sea level. This procedure produced the best results in terms of accuracy, stability and numerical efficiency. The noise level in the geoidal heights was about the same as for the second approach for low flight heights but was less by a factor of two for larger flight levels; the bias was nearly independent of flight heights between 2 and 6 km. Further improvements of the presented approaches may be achieved by modification of the integration kernels, which is beyond the scope of this contribution.

Acknowledgements. Financial support for the presented research, provided to the first author by the Canadian GEOIDE Network of Centres of Excellence through the project 'Airborne Gravity for Exploration and Mapping' and to the second author by the German Research Foundation (DFG), is gratefully acknowledged. The authors wish to thank Prof. Klaus-Peter Schwarz and Mr. Michael Kern for inspiring discussions while they stayed at the University of Calgary. Professor W. Keller, Dr. C.J. Swain and other anonymous reviewers are acknowledged for their thoughtful comments.

References

- Heiskanen WA, Moritz H (1967) Physical geodesy. Freeman, San Francisco
- Huestis SP, Parker RL (1979) Upward and downward continuation as inverse problems. *Geophys J Roy Astron Soc* 57: 171–188
- Kellogg OD (1929) Foundations of potential theory. Springer, Berlin Heidelberg New York
- Lemoine FG, Kenyon SC, Factor JK, Trimmer RG, Pavlis NK, Chinn DS, Cox CM, Klosko SM, Luthcke SB, Torrence MH, Wang YM, Williamson RG, Pavlis EC, Rapp RH, Olson TR (1998) The development of the joint NASA GSFC and NIMA geopotential model EGM96. NASA/TP-1998-206861. NASA, GSFC, Greenbelt, Maryland
- Martinec Z (1998) Boundary-value problems for gravimetric determination of a precise geoid. Lecture notes in Earth Sciences 73. Springer, Berlin Heidelberg New York
- Molodenskij MS, Eremeev VF, Yurkina MI (1960) Methods for study of the external gravitational field and figure of the Earth [translated from Russian by the Israel program for scientific translations, Office of Technical Services, Department of Commerce, Washington, DC, 1962]
- Novák P, Kern M, Schwarz KP, Heck B (2001) On the determination of a band-limited gravimetric geoid from airborne gravimetry. UCGE Tech Rep 30013, The University of Calgary
- Paul M (1973) A method of evaluation the truncation error coefficients for geoidal heights. *Bull Géod* 110: 413–425
- Sansò F (1995) The long road from the measurements to boundary value problems of physical geodesy. *Manuscr Geod* 20: 326–344
- Sjöberg LE (2001) The effect of downward continuation of gravity anomaly to sea level in Stokes' formula. *J Geod* 74: 796–804
- Vaniček P, Sun W, Ong P, Martinec Z, Najafi N, Vajda P, Ter Horst B (1996) Downward continuation of Helmert's gravity. *J Geod* 71: 21–34
- Wenzel G (1998) Ultra-high degree geopotential models GPM98 A, B, and C to degree 1800. Proc of the joint meeting Int Gravity Commission and Int Geoid Commission, Trieste, 7–12 September. (<http://www.gik.uni-karlsruhe.de/~wenzel/papers.htm>)